Article

Stem Water Potential Monitoring in Pear Orchards through WorldView-2 Multispectral Imagery

Jonathan Van Beek [1],*, Laurent Tits [1], Ben Somers [2] and Pol Coppin [1]

[1] Department of Biosystems, Katholieke Universiteit Leuven, M3-BIORES, Willem de Croylaan 34, BE-3001 Leuven, Belgium; E-Mails: laurent.tits@biw.kuleuven.be (L.T.); pol.coppin@biw.kuleuven.be (P.C.)

[2] Division Forest, Nature and Landscape, Katholieke Universiteit Leuven, Celestijnenlaan 200E, BE-3001 Leuven, Belgium; E-Mail: ben.somers@ees.kuleuven.be

* Author to whom correspondence should be addressed; E-Mail: jonathan.vanbeek@biw.kuleuven.be; Tel.: +32-1632-8146; Fax: +32-1632-2966.

Abstract: Remote sensing can provide good alternatives for traditional *in situ* water status measurements in orchard crops, such as stem water potential (Ψ_{stem}). However, the heterogeneity of these cropping systems causes significant differences with regards to remote sensing products within one orchard and between orchards. In this study, robust spectral indicators of Ψ_{stem} were sought after, independent of sensor viewing geometry, orchard architecture and management. To this end, Ψ_{stem} was monitored throughout three consecutive growing seasons in (deficit) irrigated and rainfed pear orchards and related to spectral observations of leaves, canopies and WorldView-2 imagery. On a leaf and canopy level, high correlations were observed between the shortwave infrared reflectance and *in situ* measured Ψ_{stem}. Additionally, for canopy measurements, visible and near-infrared wavelengths (R_{530}/R_{600}, R_{530}/R_{700} and R_{720}/R_{800}) showed significant correlations. Therefore, the Red-edge Normalized Difference Vegetation Index (ReNDVI) was applied on fully sunlit satellite imagery and found strongly related with Ψ_{stem} ($R^2 = 0.47$; RMSE = 0.36 MPa), undoubtedly showing the potential of WorldView-2 to monitor water stress in pear orchards. The relationship between ReNDVI and Ψ_{stem} was independent of management, irrigation setup, phenology and environmental conditions. In addition, results showed that this relation was also independent of off-nadir viewing angle and almost independent of viewing geometry, as the correlation decreased after the inclusion of fully shaded scenes.

With further research focusing on issues related to viewing geometry and shadows, high spatial water status monitoring with space borne remote sensing is achievable.

Keywords: stem water potential; multispectral imagery; robust estimation; vegetation indices; pear orchards

1. Introduction

In capital intensive cropping systems, such as pear orchards, prolonged periods of water deficiencies can lead to significant yield loss [1], making water status monitoring crucial to optimize irrigation scheduling [2]. Traditional *in situ* measurements of plant water status are time consuming and destructive, allowing only limited samples and repetitions. Furthermore, the point measurements are insufficient to account for the high spatial variability present in orchards [3]. Technological advances in remote sensing provide non-destructive, time efficient and cost beneficial alternatives that visualize the spatial variability in water status at a wide range of temporal scales [4].

Various vegetation indices have been related to leaf and canopy water content (see review by [5]). In fruit trees, however, leaf water potential (Ψ_{leaf}) has been found a more robust indicator of plant water status compared to plant water content [6,7]. Leaf water content is normally measured on tissue samples [8], which are subject to some variability, while Ψ_{leaf} provide an integrated measurement of environmental conditions on water availability within the leaf. Moreover, while large changes in leaf water content only occur at advanced stages of dehydration, Ψ_{leaf} measurements were able to detect the onset of water deficiency, allowing a reaction before permanent damage occurs [7]. Several studies have linked Ψ_{leaf} in fruit orchards with vegetation indices [9,10]. The down-side of Ψ_{leaf} is the high variability within one tree. Therefore, most researchers prefer stem water potential (Ψ_{stem}) as an indicator of plant water status in fruit orchards [7,11,12]. The Ψ_{stem} is the water status of non-transpiring leaves, which is related to the water availability and transpiration. As opposed to plant water status and Ψ_{leaf}, the potential of remote monitoring of Ψ_{stem} is not yet fully explored nor widely adopted (but see examples for olives [13] and citrus [7,14]).

Due to high cloud cover in many of the pear (and apple) growing areas of the world [15], irrigation scheduling through remote sensing requires a near-to-daily revisit time to provide the necessary information [16]. Furthermore, due to the large spatial variation within one management block [3], a high spatial resolution is required. Currently, this combination of both high spatial and temporal resolution is only feasible with high spatial resolution satellite sensors having off-nadir viewing capabilities, such as WorldView-2 (DigitalGlobe). However, most of the developed techniques and indices to monitor water status (as mentioned above) are based on reflectance information from the shortwave infrared (SWIR; 1,300–2,500 nm; [17]) and thermal infrared (3,000–35,000 nm; [18]) region of the electromagnetic spectrum. Yet very high spatial resolution satellites lack spectral bands in these regions of the spectrum. Furthermore, the highly variable off-nadir viewing angle influences spectral observations, which in turn complicates plant status monitoring [19]. Additionally, different management practices cause significant differences in orchard and tree architecture again influencing spectral observations and complicating accurate remote monitoring of plant water status [20].

This study aims at investigating the potential of WorldView-2 satellite imagery for the monitoring of Ψ_{stem}. The goal is to identify robust spectral indicators of Ψ_{stem}, independent of orchard parameters (*i.e.*, phenology, tree structure and irrigation setup), environmental conditions (*i.e.*, soil conditions) and sensor parameters (*i.e.*, off-nadir viewing angle). To this end, Ψ_{stem} was monitored throughout three consecutive growing seasons in a (deficit) irrigated and non-irrigated (rainfed) pear orchard and related to spectral observations of leaves, canopies and spectral vegetation indices derived from WorldView-2 imagery.

2. Materials and Methods

2.1. Study Area and Experimental Setup

Experiments were conducted in a (deficit) irrigated and a non-irrigated orchard, which were monitored throughout the 2011, 2012 and 2013 growing seasons.

The (deficit) irrigated orchard, planted with Conference pear trees (*Pyrus communis* L. cv. 'Conference') on Quince C rootstock, was situated in Bierbeek, Belgium (50°49'34.59"N, 4°47'42.83"E). The 2.5 m high trees were planted in 2000 in a 3.5 by 1 meter grid. They were trained in a V-system with four fruiting branches on one central stem [21]. The orchard was situated on a south-east facing slope (3.5°) with a loamy soil and two dominant row azimuths, namely 41 and 131°. The trees received 100% of the reference evapotranspiration (ETo) [22], throughout most of the growing season. In the second phenological phase, characterized by vegetative growth [23], two irrigation treatments were applied. One treatment was fully irrigated (100% ETo), while the other treatment received no irrigation from Day of Year (DOY) 150–213, to create deficit irrigation. Each treatment was applied to four adjacent rows, with all measurements performed on both center rows of each treatment to minimize the influence of adjacent rows. In each of the center rows, four plots of four trees were selected on fixed intervals (30 m) within the row. As a result, 16 plots were monitored throughout three consecutive growing seasons. Additionally, 16 fully irrigated plots with a similar management system were selected throughout the orchard and monitored throughout the growing season in 2012 and 2013. The additional plots comprise trees with different age groups, soil types and row orientation. During the experiment, all management practices were carried out without interference to the experiment.

The non-irrigated or rainfed orchard, situated in Kerkom, Belgium (50°46'24.25"N, 5°09'27.05"E), was planted in 2000 with Conference pear trees on Quince A rootstock. The 3.5 m high trees, planted in a 3.75 by 1.75 meter grid, were trained in a Spindle bush system [21]. The orchard was situated on a south facing slope (1.1°) with a loamy soil and a row azimuth of 197°. The trees were rainfed and received no additional water input. Two adjacent rows were selected and divided into eight plots of six trees, each plot consisting of four central experimental trees and two outside buffer trees. To ensure differences in water availability, root pruning was applied on one side of the canopy in the beginning of the growing season (March). In each row, a root-pruned plot was alternated with a non-treated plot.

In both orchards, the soil under the trees was kept weed free for about 0.3 m from the trunk and grass was sown in between the tree rows.

2.2. Data

2.2.1. *In Situ* Water Status

Midday stem water potential (Ψ_{stem}) was acquired for one tree per plot, on three leaves per tree, on sunny days throughout the 2011, 2012 and 2013 growing seasons (see Table 1) with a pressure chamber [24]. Prior to measurement, the leaves were covered with aluminum foil and enclosed in plastic bags to equilibrate leaf water with stem water potential [25].

Reference evapotranspiration (ETo; mm/day) was calculated according to [22] for the (deficit) irrigated and rainfed orchard from weather data obtained from nearby weather stations in Beauvechain, Belgium (50°46'49.86"N, 4°46'26.44"E) and Bierset, Belgium (50°39'18.69"N, 5°27'03.34"E), respectively.

2.2.2. Leaf Level Reflectance

Throughout the 2011, 2012 and 2013 growing seasons, leaf spectra were gathered for one tree per plot. Table 1 summarizes the exact dates of measurement. The measurements were performed with an ASD spectroradiometer (Analytic Spectral Devices, Boulder, CO, USA), conforming to [8], with a contact plant probe and an attached light source. For each tree, 20 undamaged and mature leaves were randomly selected from the sunlit part of the canopy, sampled 10 times in a basal position on the adaxial side of the leaf and averaged per leaf. All measurements were performed on sunny days within 1.5 h of local solar noon. All spectra were smoothed using a 2nd order Savitsky-Golay filter with a window size of 21 [26]. In this study, only leaf measurements coinciding with *in situ* water status measurements were considered, *i.e.*, within one day before or after a Ψ_{stem} measurement.

2.2.3. Canopy Level Reflectance

Throughout the 2011, 2012 and 2013 growing seasons, canopy reflectance measurements were collected on cloud-free days (see Table 1), using a full range (350–2,500 nm) HR-1024 spectroradiometer (Spectra Vista Corporation, New York, NY, USA). The canopy spectra were taken from an elevated position between the rows at an average height of one meter above the top of the canopy. For each plot, eight sunlit canopy spectra were taken and averaged. All measurements were performed within 1.5 h from local solar noon, to minimize differences with regards to solar geometry and illumination. All spectra were smoothed using a 2nd order Savitsky-Golay filter with a window size of 21 [26] and atmospheric water absorption features were removed. In this study, only canopy measurements coinciding with *in situ* water status measurements were considered, *i.e.*, within one day before or after a Ψ_{stem} measurement.

2.2.4. Satellite Level Reflectance

WorldView-2 multispectral iages were acquired under different off-nadir viewing angles, with a resampled ground sampling distance of 2.0 m and a spectral resolution complying eight bands: Coastal (400–450 nm), Blue (450–510 nm), Green (510–580 nm), Yellow (585–625 nm), Red (630–690 nm), Red Edge (705–745 nm), NIR1 (Near InfraRed 1; 770–895 nm) and NIR2 (860–1,040 nm). The acquisition details for the WorldView-2 images are shown in Table 2. All images were radiometrically [27],

atmospherically [28] and geometrically corrected [29]. Additionally, the position of each plot was determined with a differential global positioning system (Trimble RTK 58000).

Table 1. Ψ_{stem}, Leaf reflectance and canopy reflectance measurements for both locations during the growing seasons of 2011, 2012 and 2013. Only reflectance measurements coinciding with *in situ* water status measurements were considered, *i.e.*, within one day of a Ψ_{stem} measurement.

Location	Year	DOY of Ψstem Measurements	DOY of Leaf Level Reflectance Measurements	DOY of Canopy Level Reflectance Measurements
(Deficit) Irrigated Orchard	2011	133, 140, 146, 167, 193, 215 and 238	214	141
	2012	145, 150, 157, 166, 178, 180, 200, 207, 214, 233 and 242	242	208 and 214
	2013	159, 166, 170, 183, 187, 194, 205, 215 and 240	159, 166, 170, 183, 187, 194, 215 and 240	195 and 214
Rainfed Orchard	2011	132, 141, 151, 179 and 214	214	178
	2012	146, 151, 171, 185, 206, 217, 223 and 236	217	146 and 207
	2013	156, 163, 193, 199, 214 and 225	156, 163, 193, 214 and 225	157 and 213

Because of the unnatural hedge shape of capital intensive pear orchards, a viewing azimuth opposite the solar azimuth would imply that only shaded area was visible. Therefore, in the first part of this study, only plots acquired on the sunlit side of the canopy were considered.

Table 2. Metadata of WorldView-2 acquisitions used in this study.

Location	Year	DOY	Off-nadir Viewing Angle (°)	Satellite Azimuth (°)	Satellite Elevation (°)
(Deficit) Irrigated Orchard	2011	214	10.8	45.9	78
	2012	148	2.7	181.1	86.7
		232	18.9	209.8	68.6
	2013	189	26.1	14.7	60.7
		214	25.6	107.9	61
Rainfed Orchard	2011	214	4.8	68.6	84.7
	2012	148	15	199.8	72.9
		232	23.7	211.1	62.9
	2013	187	28	99.1	58.2
		214	27.4	133.5	58.7

2.3. Analysis

The hyperspectral leaf and canopy measurements (Sections 2.2.2 and 2.2.3) were related with the measured Ψ_{stem} values. A normalized difference ratio (Equation (1)) was calculated for each combination of wavelengths to investigate the predictive power of all wavelengths for water status estimation.

$$\text{Normalized difference ratio} = (R_x - R_y)/(R_x + R_y)$$

(1)

with R_x and R_y, the reflectance at wavelengths on the x-axis and y-axis are represented, respectively. From this analysis, the best band combinations were selected and used to relate the multispectral satellite images (Section 2.2.4) to the measured Ψ_{stem} values. The strength of correlation was determined with the coefficient of determination (R^2; Equation (2)) and the Root Mean Squared Error (RMSE; Equation (3)), with t-statistics used to test significance of correlation ($\alpha = 0.05$).

$$R^2 = 1 - \sum (y - y_{pred})^2 \Big/ \sum (y - y_{mean})^2 \tag{2}$$

$$\text{RMSE} = \sqrt{\left(\sum (y_{pred} - y)^2 \right)} \tag{3}$$

with y the measured Ψ_{stem}; y_{pred} the predicted $\Psi_{stem,}$ and y_{mean} the average Ψ_{stem}.

3. Results

3.1. Water Status

The temporal profile of the ETo (mm/day), the measured Ψ_{stem} (MPa) and its standard deviation are shown in Figure 1.
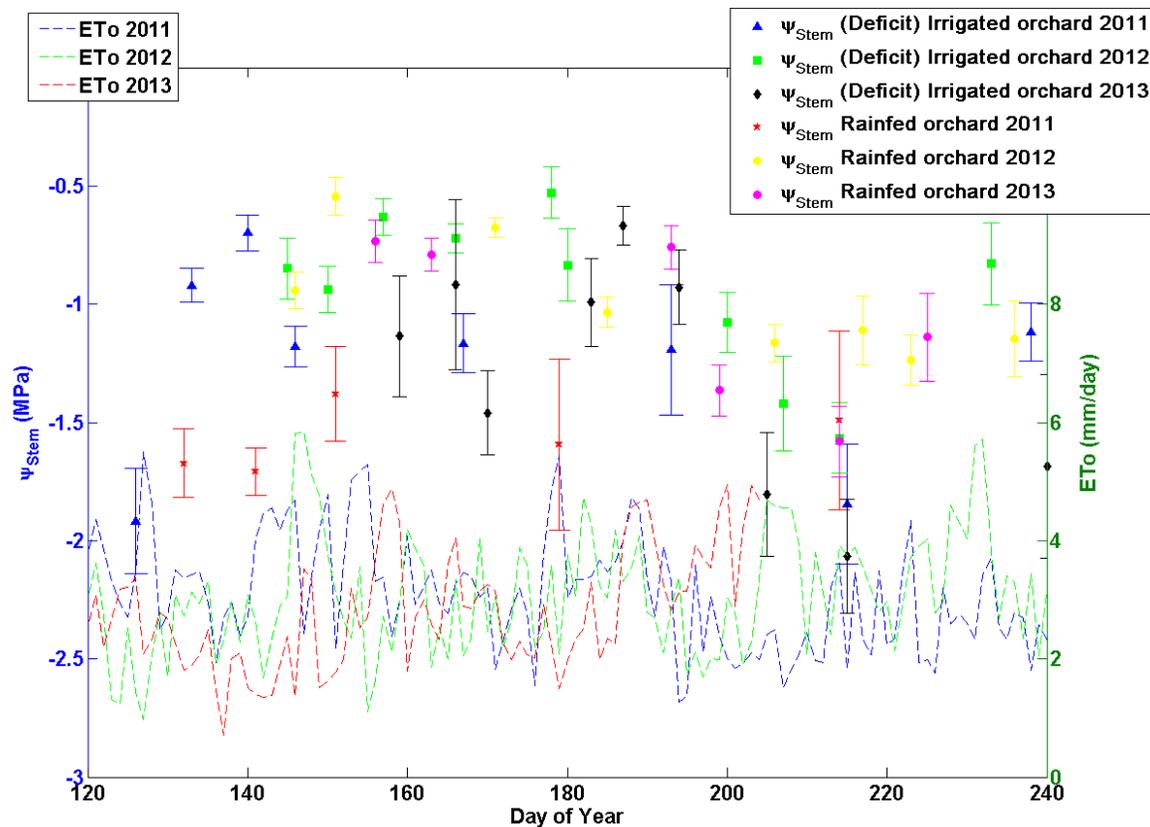
Before the experimental water treatment (DOY 150), the small standard deviations indicated similar Ψ_{stem} values within one day. Moreover, the measured Ψ_{stem} values were similar for all growing seasons and orchards pre-treatment, although a warm April and May in 2011 caused an exception.

During the water treatment, the average Ψ_{stem} values decreased and the standard deviations increased, indicative of water deficiency accumulation and differences between treatments. This effect was more pronounced in the (deficit) irrigated orchard, as a result of the larger differences between treatments. In the rainfed orchard, differences in Ψ_{stem} values throughout the growing season were less variable and more dependent on weather conditions. In general, the lowest average Ψ_{stem} values were encountered near the end of the water treatment period in the (deficit) irrigated orchard, as a result of the prolonged period of water deficiency. The extended use of drip irrigation caused small root systems [30,31], which were more sensitive to longer periods of lack of water, causing lower Ψ_{stem} values in the deficit irrigation treatment. In 2012, however, during the later stages of the experimental water treatment (DOY 180–220), ETo dropped to 2 mm/day for an extended period. Together with high rainfall (data not shown here), this caused low standard deviations and high average Ψ_{stem} values for both the (deficit) irrigated and rainfed orchard.

After the water treatment was finished, full irrigation (100% ETo) was again applied and the average Ψ_{stem} values restored to the level prior to the treatment.

As a result of the differences in experimental treatments, a wide range of Ψ_{stem} values were present in the dataset, with a slightly skewed distribution towards the lower Ψ_{stem} values. The overall average Ψ_{stem} was −1.20 MPa with a standard deviation of 0.43 MPa, a minimum value of −3.07 MPa and a maximum value of −0.42 MPa. The overall average standard deviation within each tree was 0.09 MPa (1,172 observations).

Figure 1. Reference evapotranspiration (ETo; mm/day) from Beauvechain, Belgium, and measured stem water potential (Ψ_{stem}; MPa), averaged for all plots in both the (deficit) irrigated and rainfed orchard, with bars indicating standard deviation.
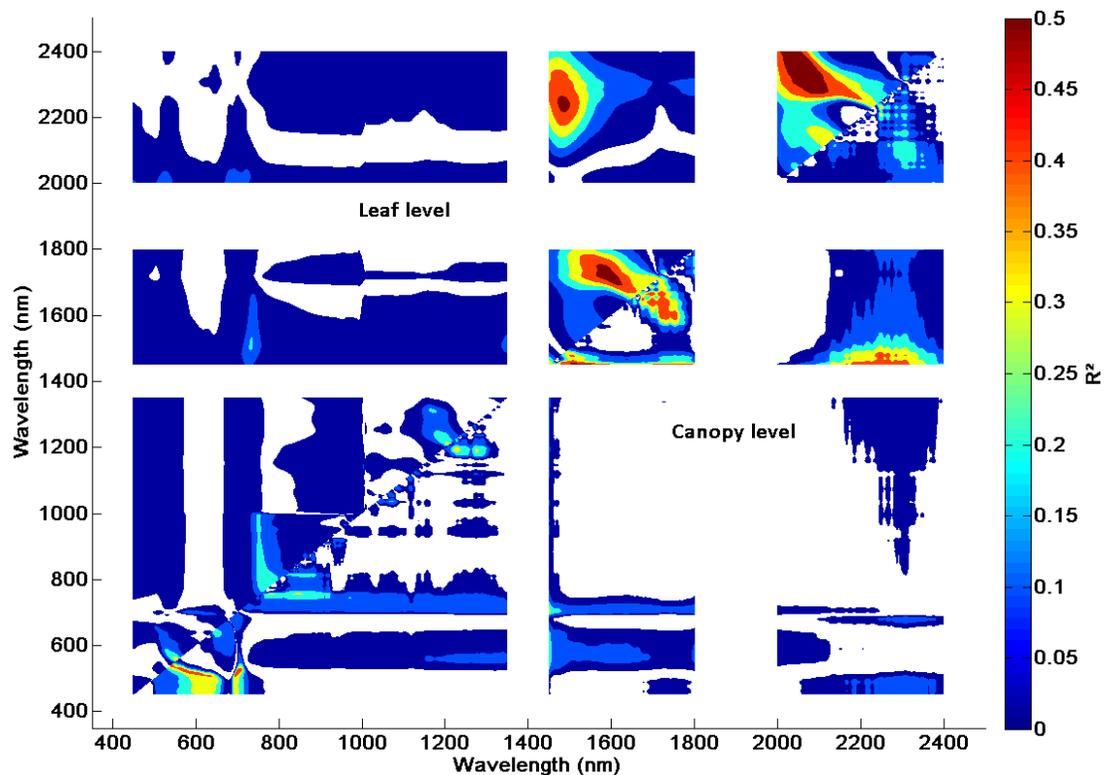

3.2. Leaf and Canopy Reflectance

Figure 2 summarizes the significant R² values between measured Ψ_{stem} and the normalized difference ratios (Equation (1)) of all wavelength combinations for both leaf (above diagonal; 395 observations; Section 2.2.2) and canopy (below diagonal; 167 observations; Section 2.2.3) reflectances.

Overall, the highest R^2 values between Ψ_{stem} and both leaf and canopy reflectance spectra ($R^2 > 0.45$) were located in the SWIR region. The R_{1400}–R_{1800} nm and R_{2000}–R_{2400} nm regions correlated strongly with Ψ_{stem} (Figure 2). Normalized difference band combinations between SWIR and other regions resulted in low(er), yet significant R^2 values. On the other hand, significant and high R^2 values were also found in the VIS-NIR region (Visible-Near Infrared; 350–1,300 nm). As the spectral range of the WorldView-2 satellite only compromised the VIS-NIR region, this was further investigated.

In the VIS-NIR region, the canopy reflectance spectra were better correlated with the Ψ_{stem} values compared to the leaf reflectance spectra (Figure 2). More specifically, several bands in the VIS-NIR region showed high R^2 values ($R^2 > 0.35$), *i.e.*, the combination of green to red (550–650 nm) or red-edge (700 nm) with blue (500–530 nm). Additionally, the combination of red-edge (700–750 nm) with NIR (800–900 nm) reflectance correlated relatively well with Ψ_{stem} ($R^2 > 0.3$). These high R^2 values were further highlighted in Figure 3, through scatterplots between Ψ_{stem} and three normalized

difference ratio indices (Equation (1)); namely, a ratio of two SWIR bands (R_{1480} and R_{2230}), a ratio of two VIS bands (R_{520} and R_{700}), and a red-edge/NIR band combination (R_{800} and R_{722}).

Figure 2. Coefficient of determination (R^2) values of normalized difference ratio of leaf measurements (above diagonal; Section 2.2.2) and canopy measurements (below diagonal; Section 2.2.3) with measured stem water potential (Ψ_{stem}; MPa) for each wavelength; only significant correlations were shown ($\alpha = 0.05$) and atmospheric water absorption bands were left out.

Similar to Figure 2, the SWIR band combination showed a high correlation with Ψ_{stem} on both leaf ($R^2 = 0.51$; RMSE = 0.34 MPa; Figure 3a) and canopy level ($R^2 = 0.39$; RMSE = 0.34 MPa; Figure 3d). The VIS combination showed a good correlation on canopy level ($R^2 = 0.48$; RMSE = 0.31 MPa; Figure 3e) but no relation on leaf level ($R^2 = 0.02$; RMSE = 0.49 MPa; Figure 3b), caused by the small range of the normalized difference ratio. Similarly, the red-edge/NIR combination showed a good correlation on canopy level ($R^2 = 0.20$; RMSE = 0.39 MPa; Figure 3f), but was incapable to estimate Ψ_{stem} on the leaf level ($R^2 = 0.04$; RMSE = 0.49 MPa; Figure 3c).

In addition to the SWIR band combinations, the canopy level showed high R^2 values in areas of the spectral domain for which the WorldView-2 sensor was also sensitive (Figures 2, 3e and 3f). The narrow regions in the VIS with high R^2 values, such as combinations between R_{600}/R_{550} and R_{700}/R_{550} (Figures 2 and 3e), might not transfer to the broad satellite bands (40–70 nm bandwidth; Section 2.2.4). In this perspective, the red-edge/NIR combination showed more potential (Figure 3f), as a result of the uniformly high R^2 values for a large region of the NIR wavelengths (750–1,000 nm), which should transfer better to broad satellite bands (Figure 2). However, both regions in the VIS/NIR

with high R^2 values indicated high potential for remote estimation of Ψ_{stem} through multispectral WorldView-2 imagery, especially since no distinctions were made between different management systems, irrigation setup and phenology.

Figure 3. (**a**–**f**) Scatter plot of normalized difference (Equation (1)) of R_{1480} and R_{2230} nm (a,d); R_{520} and R_{700} nm (b,e); R_{800} and R_{722} nm (c,f); with measured stem water potential (Ψ_{stem}; MPa). All points were labeled for location.
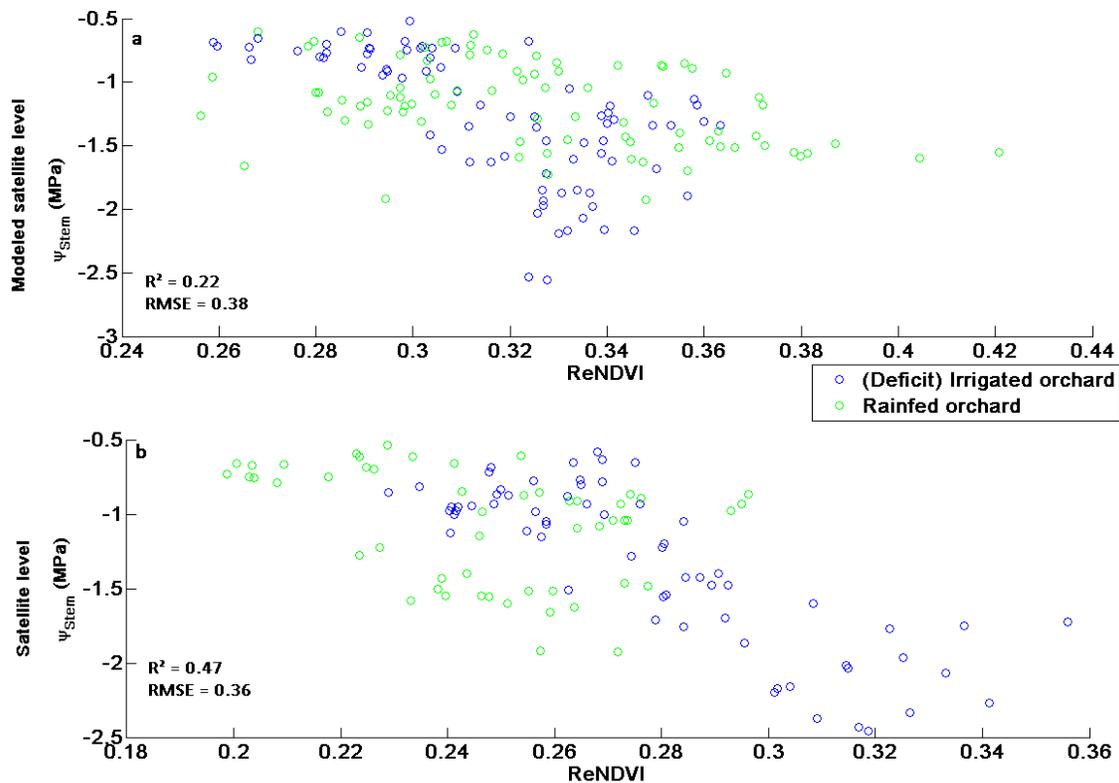

3.3. Satellite Level

As an intermediate step in the up-scaling of canopy to satellite reflectance, the canopy reflectance spectra were resampled to match the multispectral bands of the WorldView-2 satellite, using the sensor's spectral response function (similar to [32]). These were referred to as the modeled satellite level.

Based on the results of leaf and canopy level measurements (Figures 2 and 3), a set of band combinations was chosen and highlighted. The applied band combinations were based on either the red-edge/NIR region or on the blue to red region, as defined by the sensor's spectral response function [27] and the satellite bands (Section 2.2.4).

Firstly, the Red edge Normalized Difference Vegetation Index or ReNDVI (Equation (4)) was chosen, as the red edge was previously shown to be useful in the detection of plant water stress [33]. In Figure 4, the ReNDVI (Equation (4)) on a modeled satellite level and satellite level is depicted against the measured Ψ_{stem}, only Ψ_{stem} measurements closest to the acquisition were considered.

$$\text{ReNDVI} = \left(R_{NIR\ 1} - R_{Red\ Edge} \right) \big/ \left(R_{NIR\ 1} + R_{Red\ Edge} \right) \tag{4}$$

Figure 4. Scatter plot of Red edge Normalized Difference Vegetation Index (ReNDVI; Equation (4)) with measured stem water potential (Ψ_{stem}; MPa) for the modeled satellite level (**a**) and the satellite level (**b**). All points were labeled for location.

Results for the ReNDVI, in Figure 4a, showed a similar correlation between the modeled WorldView-2 reflectance and Ψ_{stem} ($R^2 = 0.22$; RMSE = 0.38 MPa) if compared to the correlation found between Ψ_{stem} and the hyperspectral (small band) ratio indices extracted from the original canopy reflectance spectra ($R^2 = 0.20$; RMSE = 0.39 MPa; Figure 3f). This was particularly interesting since this indicates the sufficient applicability of the broad spectral bands of WorldView-2 to properly monitor Ψ_{stem}. The ultimate test was the comparison between per pixel derived ReNDVI values from the actual WorldView-2 imagery and measured Ψ_{stem}. The results in Figure 4b clearly showed a similar relationship between Ψ_{stem} and ReNDVI ($R^2 = 0.47$; RMSE = 0.36 MPa), undoubtedly showing the potential of WorldView-2 to monitor water stress in pear orchards. With regards to the applicability of the index in multiple orchards, both the (deficit) irrigated and rainfed orchard showed a comparable relation with ReNDVI. However, the correlation of the rainfed orchard declined for both the modeled satellite level ($R^2 = 0.17$; RMSE = 0.30 MPa) and satellite level ($R^2 = 0.13$; RMSE = 0.36 MPa). On the other hand, the correlation of the (deficit) irrigated orchard increased for both the modeled satellite level ($R^2 = 0.41$; RMSE = 0.40 MPa) and satellite level ($R^2 = 0.67$; RMSE = 0.31 MPa). This was the result of the lower Ψ_{stem} range in the rainfed orchard.

In addition to ReNDVI, the narrow regions in the VIS region with high R^2 values (Section 3.2) were transferred into two indices, namely the Green Band Depth index (GBD; Equation (5)) and the Normalized Difference Green Blue index (Green/Blue; Equation (6)), based on the satellite bands
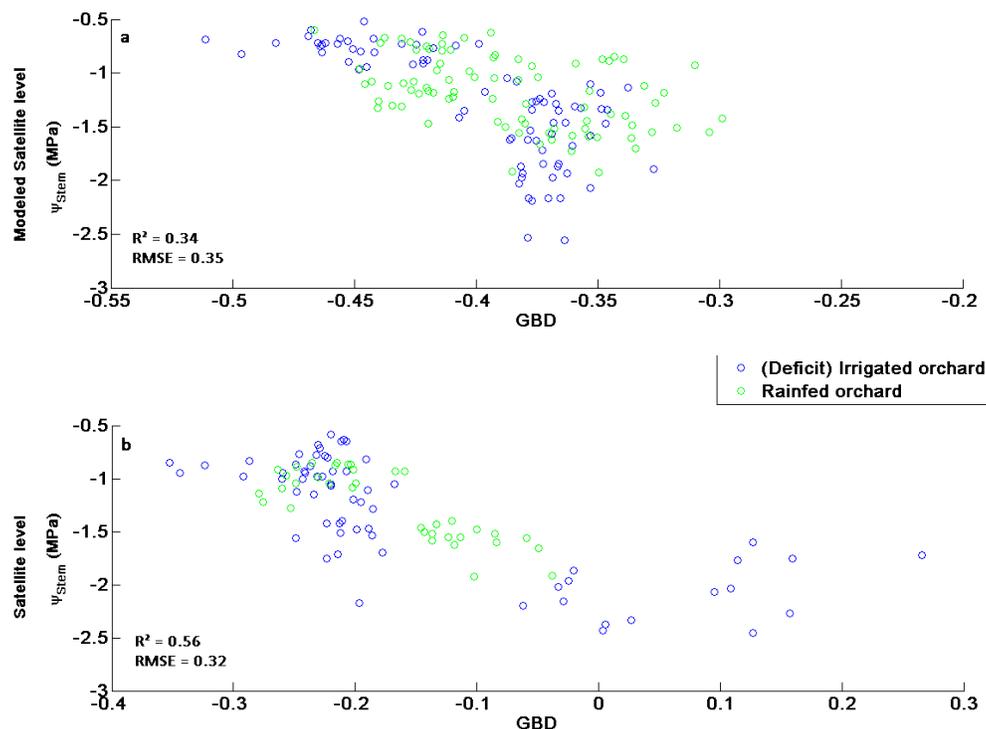
(Section 2.2.4). Similar to ReNDVI, both indices are depicted on a modeled satellite level and satellite level against measured Ψ_{stem} in Figures 5 and 6.

$$GBD = (R_{Blue} - R_{Yellow})/R_{Green} \tag{5}$$

$$Green/Blue = (R_{Green} - R_{Blue})/(R_{Green} + R_{Blue}) \tag{6}$$

The GBD (Equation (5)) showed a strong correlation on the modeled satellite level ($R^2 = 0.34$; RMSE = 0.35 MPa; Figure 5a), with similar distribution for both experimental locations. On the satellite level, the correlation was stronger ($R^2 = 0.56$; RMSE = 0.32 MPa; Figure 5b). However, Figure 5b also showed points very dissimilar to the rest of the dataset. As these effects were not present on the modeled satellite level, they were most likely caused by differences in viewing geometry.

Figure 5. Scatter plot of Green Band Depth index (GBD; Equation (5)) with measured stem water potential (Ψ_{stem}; MPa) for the modeled satellite level (**a**) and the satellite level (**b**). All points were labeled for location.
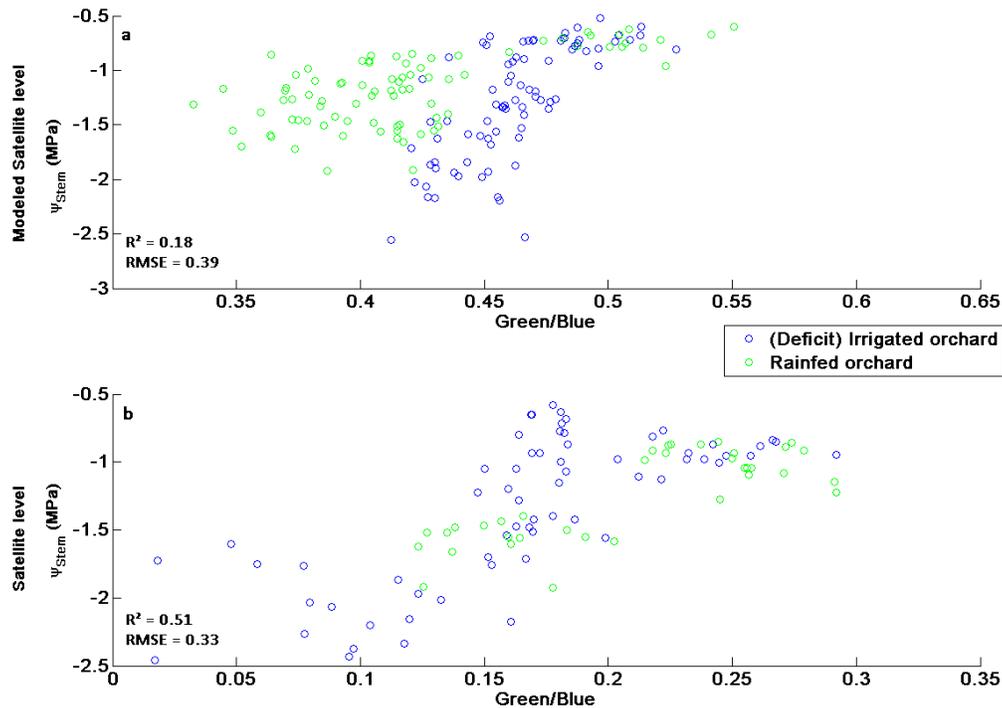

The normalized difference Green/Blue ratio (Equation (6)) also showed a strong correlation on satellite level ($R^2 = 0.51$; RMSE = 0.33 MPa; Figure 6b). However, on the modeled satellite level the differences between experimental locations were distinct and also caused a weaker correlation ($R^2 = 0.18$; RMSE = 0.39 MPa; Figure 6a). These differences were most likely the cause of different management systems (*i.e.*, the V-system and the Spindle bush, see Section 2.1).

Overall, both the GBD and the Green/Blue indices showed strong correlations on either the satellite level or the modeled satellite level but were not robust for both the satellite and modeled satellite level. Therefore, ReNDVI should be preferred for further application out of all the indices applied on a satellite level in this study, as it showed less dependence towards off-nadir viewing angle or orchard

architecture (*i.e.*, row orientation, row spacing and orchard management) on either the satellite or the modeled satellite level.

Figure 6. Scatter plot of Normalized Difference Green Blue index (Green/Blue; Equation (6)) with measured stem water potential (Ψ_{stem}; MPa) for the modeled satellite level (**a**) and the satellite level (**b**). All points were labeled for location.

4. Discussion

4.1. Potential of High Spatial and Multispectral Satellite Derived Ψ_{stem} Estimation

As could be expected, the highest R^2 values ($R^2 > 0.5$) were observed in the SWIR on the leaf level (Figure 2). Previous studies have shown the SWIR region to be affected by water absorption and thus highly correlated with leaf water content [17,34,35]. Yet, next to the SWIR region, also the VIS-NIR region showed some significant zones with high R^2 values ($R^2 > 0.2$), mostly combinations within the 740–800 nm range. Similar to the SWIR region, several studies previously showed a relation between these wavelengths and leaf water content [36–38].

On the canopy level, similar (yet less pronounced) correlations were observed between SWIR reflectance and Ψ_{stem} (Figure 2). Moreover, the VIS-NIR region of the canopy level showed higher R^2 values compared to the leaf level. This is most likely the result of the low variability in the VIS region for the leaf measurements (Figure 3b), as a consequence of the sampling design. Only mature healthy leaves were sampled, while the canopy measurements were an integrated measurement of the entire canopy (Section 2.2.3).

For canopy measurements, two regions within the VIS-NIR showed high R^2 values and potential for Ψ_{stem} estimation. On the one hand, combinations within the blue/green region were found to be strongly correlated with Ψ_{stem} (Figure 2). These band combinations were similar to the bands used by

the Photochemical Reflectance Index (PRI) [39] and are related to xanthophyll pigment changes, photosynthetic efficiency, as well providing early warning signs of water deficiency, in fruit orchards [13,14,39]. These narrow band combinations (R_{531} and R_{570}) were not applicable on the broad satellite wavebands of WorldView-2, as they were included in one band (Green; 510–580 nm).
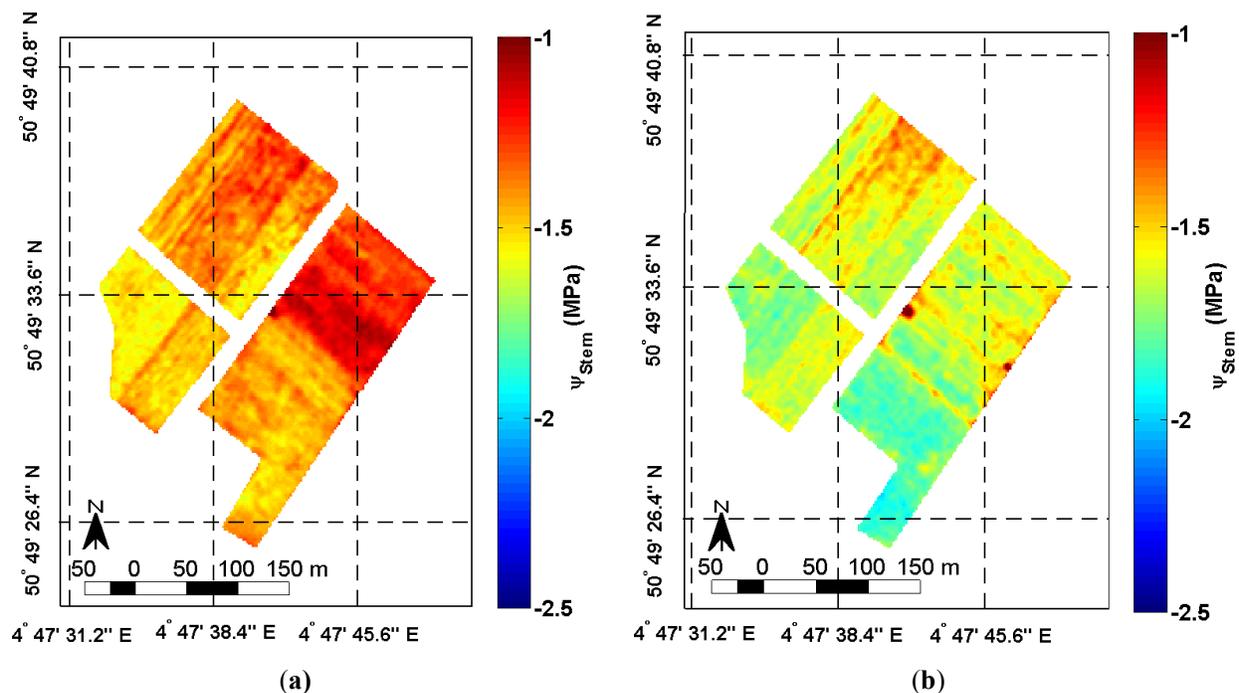
On the other hand, the combination of the red-edge (700–750 nm) with the NIR region (800–900 nm) also showed a strong correlation with Ψ_{stem} (Figure 2). Contrary to the PRI bands, the R² values remained high for a large range of wavelengths, well suited for application on the broad satellite bands (Full Width Half Maximum between 50 and 100 nm). Previous research showed the relation between the red-edge region and stress detection [13,33], especially the shape and position of the red-edge [40,41]. For healthy leaves, the red-edge inflection point showed a displacement towards the longer wavelengths as a result of high pigment concentrations [41]. However, during stressed periods and as a result of stress-induced chlorosis, the red-edge inflection point would shift to shorter wavelengths [13]. In addition to the correlation with chlorophyll content [40], the red edge was also found to be highly dependent on phenology, leaf water content and leaf area [41,42], causing lower R^2 values for the leaf measurements (Figure 2). As the resulting effect of water deficiency could be manifold, *i.e.*, changes in water content, chlorophyll content, leaf area and leaf angle [43–45], and with the red-edge sensitive to all these influences, the red-edge could provide a good estimation of the overall health and stress level of a canopy. Moreover, it should also have a high correlation with Ψ_{stem}, as this is a measurement of the integrated effect of environmental conditions on water availability within the plant. This correlation between water potential measurements and biophysical variables was also shown by [42], where strong indices for Ψ_{leaf} were also strongly correlated with leaf area related indices (*i.e.*, Normalized Difference Vegetation Index; [45]) and less with water content related indices (*i.e.*, Water Index; [46]).

Overall, our analysis of leaf and canopy reflectance indicated high potential for the mapping of Ψ_{stem} with VIS/NIR derived band combinations, especially when keeping in mind that no distinctions were made between different management systems, irrigation setup, phenology and environmental conditions. We could further demonstrate this potential using WorldView-2 imagery (Figure 4).

The ReNDVI (Equation (4)), derived from the Red-edge and NIR1 band of WorldView-2 (Section 2.2.4.), was shown to be highly dependent on Ψ_{stem} and could be used in the remote estimation hereof. As an illustration on how such ReNDVI maps could be used for steering irrigation management, Figure 7 shows the index maps converted to estimates of Ψ_{stem} (RMSE = 0.36 MPa) for the (deficit) irrigated orchard.

The image on the left was taken during an extended period of full irrigation, while the image on the right was taken during a deficit water experiment. The maps visualize spatial differences within each orchard block and indicate different zones in the orchard requiring different irrigation management, or the presence of problems related to obstructions in the irrigation system. In general, Ψ_{stem} readings below −1.5 MPa should be considered as a cut-off between moderate and severe water stress levels [1]. As expected, due to irrigation, Figure 7a showed no severely stressed trees (red to orange colors), while Figure 7b, acquired during a water stress experiment, showed large differences between different management blocks and water deficiency in some blocks (blue colors). With regular Ψ_{stem} maps throughout the growing season, irrigation scheduling with remote sensing input becomes feasible.

Figure 7. Stem water potential (Ψ_{stem}) map (MPa) of the (deficit) irrigated orchard based on the correlation depicted in Figure 4 ($R^2 = 0.47$; RMSE = 0.36 MPa), for the image taken in 2012 on Day Of the Year (DOY) 232 (**a**) and the image taken in 2013 on DOY 189 (**b**) Based on the correlation between satellite derived Red edge Normalized Difference Vegetation Index (ReNDVI, Equation (4)) and measured Ψ_{stem} ($R^2 = 0.47$; RMSE = 0.36 MPa; Figure 4), a Ψ_{stem} map was derived. To avoid effects related to the canopy discontinuity, as a result of the alternation between canopies, shadows and grasses, a 3×3 pixel moving-average filter was applied. The filtering operation smoothed the image and facilitated visual interpretation, in similar fashion to [9].
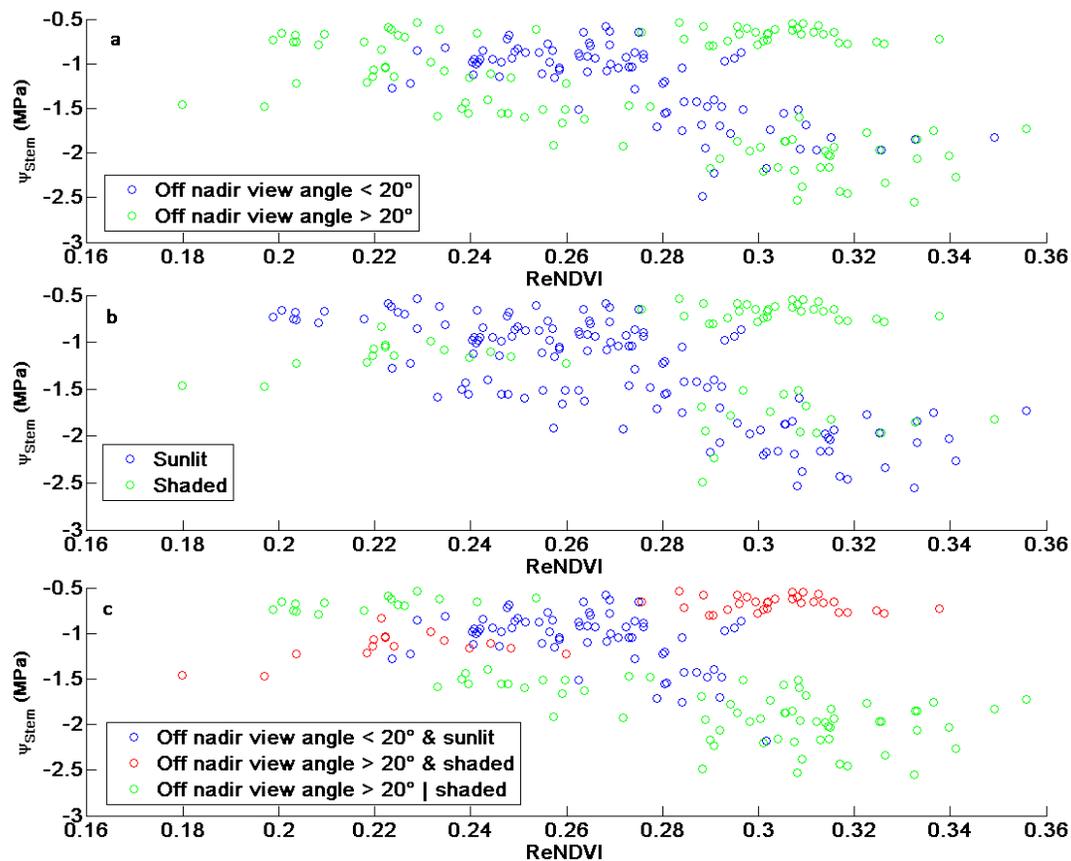

(**a**)   (**b**)

4.2. Limitations of High Spatial and Multispectral Satellite Imagery

In this study, no distinction was made between different management systems, irrigation setup, phenology and location, and still we could demonstrate the robustness of the WorldView-2 derived ReNDVI in estimating Ψ_{stem}. However, so far we only incorporated imagery with a viewing angle that allowed fully sunlit canopies. The distinction between sunlit and shaded scenes was based on the difference between the row azimuth and the relative azimuth between sensor and sun. Other studies have shown that the inclusion of shaded canopy parts could cause a decrease in correlation [13,14]. In Figure 8, all the acquired images (Table 2) were taken into account, including imagery with different viewing geometry.

Similar to other studies [13,14], the predictive power of the ReNDVI decreased after the inclusion of all the shaded scenes, as is shown in Figure 8 ($R^2 = 0.18$; RMSE = 0.49 MPa). On the other hand, Figure 8a,b also showed a clear influence of viewing geometry on the ReNDVI index value. In addition to the light conditions in the plot, namely sunlit or shaded canopy, the off-nadir viewing angle was also shown to be important. The ReNDVI was only affected by the combination of high

off-nadir viewing angles (*i.e.*, off-nadir viewing angles over 20°) and a viewing geometry opposite to the sun with regards to the rows. The relative position of the sensor was important for larger off-nadir viewing angles (>20°), as it determined whether the scene was fully sunlit or fully shaded. However, for smaller off-nadir viewing angles (<20°), the relative position of the sensor with regards to the sun and row orientation was found not to be important, as most of the canopy would still be sunlit. With the shaded scenes with small off-nadir viewing angles (<20°), the R^2 increased to 0.56 and RMSE remained at 0.36 MPa (Figure 8c).

Figure 8. Red edge Normalized Difference Vegetation Index (ReNDVI; Equation (4)) against measured stem water potential (Ψ_{stem}; MPa) for the satellite level, labeled for off-nadir viewing angle of the sensor (**a**), scene light conditions based on the sensor's relative azimuth (**b**) and a combination of both (**c**).

One influential parameter that could hamper applicability of the ReNDVI index is the background, *i.e.*, the bare soil, cover crop or shadow. The influence of background on the use of the ReNDVI was not investigated here, as both the (deficit) irrigated and rainfed orchard had grass sown in between the rows to minimize soil erosion. However, some researchers have already indicated that soil background effects could decrease the correlation between vegetation indices and biophysical variables [14,47].

Ongoing research is focusing on developing and applying specific spectral mixture analysis techniques [48–50] to address these issues. As such, we hope to further advance the operational implementation of high resolution multispectral satellite observations, such as WorldView-2, in

precision agriculture. The results presented in this work show great promise for the remote steering of irrigation management.

5. Conclusions

This study aimed at investigating the potential of WorldView-2 satellite imagery for monitoring of stem water potential (Ψ_{stem}). To this end, Ψ_{stem} was monitored throughout three consecutive growing seasons in a (deficit) irrigated and non-irrigated (rainfed) pear orchard and related to spectral observations of leaves, canopies and WorldView-2 satellite imagery. Through ground measurements of leaf and canopy level, a robust spectral indicator of Ψ_{stem} was sought, independent of orchard parameters (*i.e.*, phenology, tree structure and irrigation setup) and environmental conditions (*i.e.*, soil conditions). Through satellite imagery, the sensitivity of the spectral indicator towards sensor parameters (*i.e.*, off-nadir view angle, viewing geometry) was investigated.

For hyperspectral ground measurements, it was shown that next to the Shortwave Infrared Region (SWIR) (combinations of the reflectance at 1,430 nm (R_{1430}) and R_{2230}), also the Visible-Near Infrared Region (VIS-NIR) showed regions with significant R^2 values for leaf level measurements. This was more pronounced at canopy level, for which combinations within the blue/green region (R_{500} to R_{570}) together with the red/red-edge region (R_{670} to R_{720}) were strongly related to Ψ_{stem}. Yet, the combinations of the red-edge (R_{700} to R_{750}) with the NIR region (R_{800} to R_{900}) were more suited for application on the broad satellite bands, as they showed a strong correlation with Ψ_{stem} for a larger range of wavelengths for both leaf and canopy level.

The Red-edge Normalized Difference Vegetation Index (ReNDVI), derived from the Red-edge (705–745 nm) and NIR1 (Near InfraRed 1; 770–895 nm) band of WorldView-2, was shown to be highly dependent on Ψ_{stem} and could be used in the remote estimation hereof, independent of management systems, irrigation setup, phenology and environmental conditions. In addition, results showed that the relation between Ψ_{stem} and ReNDVI was independent of the off-nadir viewing angle and almost independent of viewing geometry. For larger off-nadir viewing angles, the relative position of the sensor determined whether the scene was fully sunlit or fully shaded, while for smaller off-nadir viewing angles the scene would be mostly sunlit, independent on the azimuth of the sensor. With the inclusion of these partly shaded but mostly sunlit scenes, the correlation improved ($R^2 = 0.56$; RMSE = 0.36 MPa).

With further research focusing on issues related to viewing geometry and shadows, high spatial water status monitoring with space borne remote sensing is achievable.

Acknowledgments

Conflicts of Interest

The authors declare no conflict of interest.

References

1. Janssens, P.; Deckers, T.; Elsen, F.; Elsen, A.; Schoofs, H.; Verjans, W.; Vandendriessche, H. Sensitivity of root pruned 'Conference' pear to water deficit in a temperate climate. *Agric. Water Manag.* **2011**, *99*, 58–66.
2. Pinter, P.J., Jr.; Hatfield, J.L.; Schepers, J.S.; Barnes, E.M.; Moran, M.S.; Daughtry, C.S.T.; Upchurch, D.R. Remote sensing for crop management. *Photogramm. Eng. Remote Sens.* **2003**, *69*, doi:10.14358/PERS.69.6.647.
3. Perry, E.M.; Dezzani, R.J.; Seavert, C.F.; Pierce, F.J. Spatial variation in tree characteristics and yield in a pear orchard. *Precis. Agric.* **2010**, *11*, 42–60.
4. Dorigo, W.A.; Zurita-Milla, R.; de Wit, A.J.W.; Brazile, J.; Singh, R.; Schaepman, M.E. A review on reflective remote sensing and data assimilation techniques for enhanced agroecosystem modeling. *Int. J. Appl. Earth Obs. Geoinf.* **2007**, *9*, 165–193.
5. Govender, M.; Dye, P.J.; Weiersbye, I.M.; Witkowski, E.T.F.; Ahmed, F. Review of commonly used remote sensing and ground-based technologies to measure plant water stress. *Water SA* **2009**, *35*, 741–752.
6. Sepulcre-Canto, G.; Zarco-Tejada, P.J.; Jimenez-Munoz, J.C.; Sobrino, J.A.; Soriano, M.A.; Fereres, E.; Vega, V.; Pastor, M. Monitoring yield and fruit quality parameters in open-canopy tree crops under water stress. Implications for ASTER. *Remote Sens. Environ.* **2007**, *107*, 455–470.
7. Dzikiti, S.; Verreynne, J.S.; Stuckens, J.; Strever, A.; Verstraeten, W.W.; Swennen, R.; Coppin, P. Determining the water status of Satsuma mandarin trees [*Citrus Unshiu Marcovitch*] using spectral indices and by combining hyperspectral and physiological data. *Agric. For. Meteorol.* **2010**, *150*, 369–379.
8. Stuckens, J.; Verstraeten, W.W.; Delalieux, S.; Swennen, R.; Coppin, P. A dorsiventral leaf radiative transfer model: Development, validation and improved model inversion techniques. *Remote Sens. Environ.* **2009**, *113*, 2560–2573.
9. Acevedo-Opazo, C.; Tisseyre, B.; Guillaume, S.; Ojeda, H. The potential of high spatial resolution information to define within-vineyard zones related to vine water status. *Precis. Agric.* **2008**, *9*, 285–302.
10. Serrano, L.; González-Flor, C.; Gorchs, G. Assessment of grape yield and composition using the reflectance based Water Index in Mediterranean rainfed vineyards. *Remote Sens. Environ.* **2012**, *118*, 249–258.
11. Naor, A.; Gal, Y.; Peres, M. The inherent variability of water stress indicators in apple, nectarine and pear orchards, and the validity of a leaf-selection procedure for water potential measurements. *Irrig. Sci.* **2006**, *24*, 129–135.
12. McCutchan, H.; Shackel, K.A. Stem-water potential as a sensitive indicator of water stress in prune trees (*Prunus domestica* L. cv. French). *J. Am. Soc. Hortic. Sci.* **1992**, *117*, 607–611.

13. Suárez, L.; Zarco-Tejada, P.J.; Sepulcre-Cantó, G.; Pérez-Priego, O.; Miller, J.R.; Jiménez-Muñoz, J.C.; Sobrino, J. Assessing canopy PRI for water stress detection with diurnal airborne imagery. *Remote Sens. Environ.* **2008**, *112*, 560–575.

14. Stagakis, S.; González-Dugo, V.; Cid, P.; Guillén-Climent, M.L.; Zarco-Tejada, P.J. Monitoring water stress and fruit quality in an orange orchard under regulated deficit irrigation using narrow-band structural and physiological remote sensing indices. *ISPRS J. Photogramm. Remote Sens.* **2012**, *71*, 47–61.

15. Marshall, G.J.; Dowdeswell, J.A.; Rees, W.G. The spatial and temporal effect of cloud cover on the acquisition of high quality landsat imagery in the european arctic sector. *Remote Sens. Environ.* **1994**, *50*, 149–160.

16. Moran, M.S.; Fitzgerald, G.J.; Rango, A.; Walthall, C.L.; Barnes, E.D.; Bausch, W.C.; Clarke, T.R.; Daughtry, C.S.; Everitt, J.H..; Hatfield, J.L.; *et.al.* Sensor development and radiometric correction for agricultural applications. *Photogramm. Eng. Remote Sens.* **2003**, *69*, 705–718.

17. Ceccato, P.; Flasse, S.; Grégoire, J.-M. Designing a spectral index to estimate vegetation water content from remote sensing data: Part 2. Validation and applications. *Remote Sens. Environ.* **2002**, *82*, 198–207.

18. Jackson, R.D.; Idso, S.B.; Reginato, R.J.; Pinter, P.J., Jr. Canopy temperature as a crop water stress indicator. *Water Resour. Res.* **1981**, *17*, 1133–1138.

19. Zhao, F.; Gu, X.; Verhoef, W.; Wang, Q.; Yu, T.; Liu, Q., Huang, H.; Qin, W.; Chen, L.; Zhao, H. A spectral directional reflectance model of row crops. *Remote Sens. Environ.* **2010**, *114*, 265–285.

20. Haboudane, D.; Miller, J.R.; Pattey, E.; Zarco-Tejada, P.J.; Strachan, I.B. Hyperspectral vegetation indices and novel algorithms for predicting green LAI of crop canopies: Modeling and validation in the context of precision agriculture. *Remote Sens. Environ.* **2004**, *90*, 337–352.

21. Sansavini, S.; Musacchi, S. Canopy architecture, training and pruning in the Modern European pear orchards: An overview. *Acta Hort.* **1994**, *367*, 152–172.

22. Allen, R.G.; Pereira, L.S.; Raes, D.; Smith, M. *Crop Evapotranspiration—Guidelines for Computing Crop Water Requirements—FAO Irrigation and Drainage Paper 56*; Food and Agriculture Organization of the United Nations: Rome, Italy, 1998.

23. Mitchell, P.D.; Jerie, P.H.; Chalmers, D.J. Effects of regulated water deficits on pear tree growth, flowering, fruit growth, and yield. *J. Am. Soc. Hortic. Sci.* **1984**, *109*, 604–606.

24. Scholander, P.F.; Bradstreet, E.D.; Hemmingsen, E.A.; Hammel, H.T. Sap pressure in vascular plants. *Science* **1965**, *148*, 339–346.

25. Begg, J.E.; Turner, N.C. Water potential gradients in field tobacco. *Plant Physiol.* **1970**, *46*, 343–346.

26. Savitsky, A.; Golay, M.J.E. Smoothing and differentiation of data by simplified least squares procedures. *Anal. Chem.* **1964**, *36*, 1627–1639.

27. Radiometric Use of WorldView-2 Imagery. Available online: http://www.digitalglobe.com/sites/default/files/Radiometric_Use_of_WorldView-2_Imagery%20%281%29.pdf (accessed on 3 December 2013).

28. Adler-Golden, S.; Berk, A.; Bernstein, L.S.; Richtsmeier, S.; Acharya, P.K.; Matthew, M.W.; Anderson, G.P.; Allred, C.L.; Jeong, L.S.; Chetwynd, J.H. Flaash, a Modtran4 Atmospheric Correction Package for Hyperspectral Data Retrievals and Simulations. In *Summaries of the Seventh JPL Airborne Earth Science Workshop January 12–16, 1998*; Jet Propulsion Laboratory, National Aeronautics and Space Administration: Pasadena, CA, USA, 1998.

29. Grodecki, J.; Dial, G. Block adjustment of high-resolution satellite images described by rational polynomials. *Photogramm. Eng. Remote Sens.* **2003**, *69*, doi:10.14358/PERS.69.1.59.

30. Araujo, F.; Williams, L.E.; Grimes, D.W.; Matthews, M.A. A comparative study of young 'Thompson Seedless' grapevines under drip and furrow irrigation. I. Root and soil water distributions. *Sci. Hortic.* **1995**, *60*, 235–249.

31. Fernandez, J.E.; Moreno, F.; Cabrera, F.; Arrue, J.L.; Martın-Aranda, J. Drip irrigation, soil characteristics and the root distribution and root activity of olive trees. *Plant Soil* **1991**, *133*, 239–251.

32. van Leeuwen, W.J.D.; Orr, B.J.; Marsh, S.E.; Herrmann, S.M. Multi-sensor NDVI data continuity: Uncertainties and implications for vegetation monitoring applications. *Remote Sens. Environ.* **2006**, *100*, 67–81.

33. Blackburn, G.A. Hyperspectral remote sensing of plant pigments. *J. Exp. Bot.* **2007**, *58*, 855–67.

34. Ceccato, P.; Flasse, S.; Tarantola, S.; Jacquemoud, S.; Grégoire, J.-M. Detecting vegetation leaf water content using reflectance in the optical domain. *Remote Sens. Environ.* **2001**, *77*, 22–33.

35. Gao, B. NDWI—A normalized difference water index for remote sensing of vegetation liquid water from space. *Remote Sens. Environ.* **1996**, *58*, 257–266.

36. Hunt, E.R., Jr; Rock, B.N. Detection of changes in leaf water content using Near- and Middle-infrared reflectances. *Remote Sens. Environ.* **1989**, *30*, 43–54.

37. Danson, F.M.; Steven, M.D.; Malthus, T.J.; Clark, J.A. High-spectral resolution data for determining leaf water content. *Int. J. Remote Sens.* **1992**, *13*, 461–470.

38. Mogensen, V.O.; Jensen, C.R.; Mortensen, G.; Thage, J.H.; Koribidis, J.; Ahmed, A. Spectral reflectance index as an indicator of drought of field grown oilseed rape (*Brassica napus* L.). *Eur. J. Agron.* **1996**, *5*, 125–135.

39. Gamon, J.A.; Serrano, L.; Surfus, J.S. The photochemical reflectance index : An optical indicator of photosynthetic radiation use efficiency across species, functional types, and nutrient levels. *Oecologia* **1997**, *112*, 492–501.

40. Blackburn, G.A. Relationships between spectral reflectance and pigment concentrations in stacks of deciduous broadleaves. *Remote Sens. Environ.* **1999**, *70*, 224–237.

41. Horler, D.N.H.; Dockray, M.; Barber J. The red edge of plant reflectance. *Int. J. Remote Sens.* **1983**, *4*, 273–288.

42. Stagakis, S.; Markos, N.; Sykioti, O.; Kyparissis, A. Monitoring canopy biophysical and biochemical parameters in ecosystem scale using satellite hyperspectral imagery: An application on a *Phlomis fruticosa* Mediterranean ecosystem using multiangular CHRIS/PROBA observations. *Remote Sens. Environ.* **2010**, *114*, 977–994.

43. Lakso, A.N. The effects of water stress on physiological processes in fruit crops. *Acta Hort.* **1984**, *171*, 275–290.

44. Guerfel, M.; Baccouri, O.; Boujnah, D.; Chaïbi, W.; Zarrouk, M. Impacts of water stress on gas exchange, water relations, chlorophyll content and leaf structure in the two main Tunisian olive (*Olea europaea* L.) cultivars. *Sci. Hortic.* **2009**, *119*, 257–263.

45. Haas, R.H.; Schell, J.A. *Monitoring the Vernal Advancement and Retrogradation (greenwave Effect) of Natural Vegetation*; Remote Sensing Center, Texas A & M University: Denton, TX, USA, 1974.

46. Penuelas, J.; Filella, I.; Biel, C.; Serrano, L.; Savé, R. The reflectance at the 950–970 nm region as an indicator of plant water status. *Int. J. Remote Sens.* **1993**, *14*, 1887–1905.

47. Zarco-Tejada, P.J.; Miller, J.R.; Morales, A.; Berjón, A.; Agüera, J. Hyperspectral indices and model simulation for chlorophyll estimation in open-canopy tree crops. *Remote Sens. Environ.* **2004**, *90*, 463–476.

48. Somers, B.; Delalieux, S.; Verstraeten, W.; Coppin, P. A conceptual framework for the simultaneous extraction of sub-pixel spatial extent and spectral characteristics of crops. *Photogramm. Eng. Remote Sens.* **2009**, *75*, 57–68.

49. Tits, L.; Somers, B.; Stuckens, J.; Farifteh, J.; Coppin, P. Integration of *in situ* measured soil status and remotely sensed hyperspectral data to improve plant production system monitoring: Concept, perspectives and limitations. *Remote Sens. Environ.* **2013**, *128*, 197–211.

50. Iordache, D.-M.; Tits, L.; Plaza, A.; Bioucas-Dias, J.; Somers, B. A dynamic unmixing framework for site specific monitoring of plant production systems. *IEEE J. Sel. Top. Appl. Earth Obs. Remote Sens.* **2013**, submitted.